Colloids and Surfaces, 64 (1992) 245–264
Elsevier Science Publishers B.V., Amsterdam

Contribution of ionic correlations to excess free energy and disjoining pressure of thin liquid films 1. Electric double layer inside the film

Peter A. Kralchevsky and Vesselin N. Paunov
Laboratory of Thermodynamics and Physico-Chemical Hydrodynamics, Faculty of Chemistry, University of Sofia, Sofia 1126, Bulgaria

(Received 5 November 1991; accepted 28 January 1992)

Abstract

An approach to the calculation of the ionic-correlation free energy per unit area of thin liquid films is developed. The Poisson–Boltzmann ion charge distribution inside the film is replaced by an equivalent stepwise model distribution. In this way comparatively simple expressions for calculating the correlation free energy and disjoining pressure are derived. The results are in good agreement with numerical data of other authors. The dependence of the ionic-correlation free energy on various factors (dielectric permittivities, width of the Stern layer, electrolyte concentration, ionic charge, surface charge density, temperature) is examined. In all cases the ionic correlations give rise to an attractive contribution to the disjoining pressure, which often exceeds the contribution due to the van der Waals forces. In the case of 2:2 electrolytes the combined action of ionic correlations and van der Waals attraction can prevail over the electrostatic repulsion and a net attraction between the two film surfaces takes place.

Keywords: Disjoining pressure, excess free energy: ionic correlations; thin liquid films.

1. Introduction

In spite of the fact that the Derjaguin–Landau–Verwey–Overbeek (DLVO) theory was found to be the main theoretical concept in the field of colloid stability [1–5], this theory often does not exhibit good agreement with experiment. For example, unreasonably large values of the Hamaker constant ($A_H \sim 10^{-19}$ J) are needed for interpreting the data from coagulation of colloids [6,7].

The existing problems about the agreement between theory and experiment can be overcome, at least in part, if the effects of the ionic correlations in the electric double layers are taken into account. Debye and Hückel [8] were the first who accounted for the contribution of the ionic correlations in the free energy of uniform electrolyte solutions. Considerably later, ionic correlations in non-uniform and non-isotropic solutions were studied. Martynov [9] considered the contribution of the ionic correlations and image forces into capacitance of an electric double layer. His approach was based on the Bogolyubov–Born–Green–Yvon set of equations for the correlation functions. Later Outhwaite and co-workers [10–12] treated the same problem by means of the hypernetted chain (HNC) equation. Another approach is based on computer simulations, see for example Refs [13 and 14].

In the case of two overlapping electric double layers (a thin film), ionic correlations contribute to the disjoining pressure of the thin film. To calculate

Correspondence to: P.A. Kralchevsky, Laboratory of Thermodynamics and Physico-Chemical Hydrodynamics, Faculty of Chemistry, University of Sofia, Sofia 1126, Bulgaria.

0166-6622/92/$05.00

the respective contributions, Derjaguin [5] and Muller and Derjaguin [15] used a model of the counterion atmosphere. According to this model, the counterions are located on two planes, which are parallel to the respective film surfaces (Helmholtz model). These authors concluded that the ionic-correlation disjoining pressure component is comparable to the electrostatic component only at very small film thicknesses ($h \sim 2$ nm). However, at such small film separations the finite size of the ions should also be taken into account. In the case of an electrolyte film between two uncharged surfaces, ionic-correlation effects were studied by Gorelkin and Smilga [16], Mitchell and Richmond [17], Richmond [18,19], and Carnie and Chan [20].

In the case of charged film surfaces the situation is more complicated because of the non-uniform distribution of the ions inside the film. In this case quantitative results were obtained by Guldbrand et al. [21] by means of the Monte Carlo method. These authors established the following two effects due to ionic correlations. (i) The ions are located closer to the film surfaces, which results in a decreased overlapping of the two counterion atmospheres; (ii) the ionic correlations give rise to attractive forces, similar to the van der Waals forces. Under some conditions the net attractive force can exceed the electrostatic repulsion.

An alternative approach to the correlation effects in thin films was proposed by Kjellander and Marčelja [22]. They developed a computer method for solving the integral equations of the statistical mechanics in the framework of the HNC-closure. They studied separately the cases without electrolyte [23] and with electrolyte [24]. These authors found that in some cases the effect of the ionic correlations inside the film can be accounted for by using the conventional DLVO theory with an effective surface charge lower than the real one [24].

An alternative to the above numerical methods was proposed by Attard et al. [25,26], who developed an analytical approach called the Extended Poisson–Boltzmann theory (EPB). This approach allows calculation of the excess film free energy and disjoining pressure from the ionic charge density distribution inside the film. In particular, for solutions without electrolyte they obtained a correlation disjoining pressure $\Pi_{cor} \sim h^{-2}$ for large film thickness h [25]. Exponential decay of Π_{cor} was established for electrolyte-containing solutions [26]. In spite of its elegant form, the EPB theory is not easy to apply numerically because of its complex mathematics.

The numerical results show that the attractive forces due to the ionic correlations inside the thin films can be in the order of the known van der Waals forces, and even larger. However, as a rule, the effect of ionic correlations is not taken into account when interpreting experimental data for disjoining pressure or contact angles, see for example Refs [3,27 and 28]. We believe this situation is due, at least in part, to the complicated and inaccessible form of the existing theories of the ionic-correlation disjoining pressure. That is why our aim in the present study is to develop a conceptually and mathematically simpler approach to the ionic correlations in thin liquid films at the cost of some model simplifications. Such a model approach is possible because the excess correlation free energy is an integral of the respective free energy density between the thin film surfaces. Then one can replace the real continuous charge density distribution inside the film (expressed by elliptical functions) by an appropriate simple stepwise model distribution. Fortunately this model approach turns out to give not only simpler expressions but also numerically correct results (see Section 5 below).

This paper is organized as follows. Section 2 presents the theoretical method. The model of the charge density distribution is introduced in Section 3 and the calculation of the correlation internal and free energies is described in Section 4. Electrolyte-containing films between two similar dielectrics as well as conductor phases are considered. The effect of different factors (electrolyte concentration, surface charge density, dielectric permittivities, Stern layer, etc.) on the ionic-correlation

disjoining pressure is examined in Section 5. Appendix A contains derivations of some equations, whereas Appendix B presents the algorithm for computer calculations.

As mentioned above, the present paper deals with electrolyte-containing films, i.e. electric double layers are present inside the film. This is the case for foams, suspensions, or oil-in-water emulsions. The ionic-correlation effects in water-in-oil emulsions, where the electric double layers are situated outside the liquid film, are investigated in Part 2 of this study; Ref. [29].

2. Theoretical method

Our treatment of the correlation energy is based on the equation [9,20,30]

$$\nabla^2\varphi - \kappa^2\varphi = -\frac{4\pi}{\epsilon}q\delta(\boldsymbol{r}) \tag{2.1}$$

where φ is a fluctuation polarization electrical potential due to the presence of the electrical charge q at the point $r = 0$;

$$\kappa^2 = \frac{4\pi}{\epsilon k_B T}\sum_m q_m^2 n_m(r) \tag{2.2}$$

where ϵ is dielectric permittivity, k_B is the Boltzmann constant, T is temperature, n_m is the numerical density of the mth ion species,

$$q_m = Z_m e \tag{2.3}$$

is the respective ion charge with e being the charge of the electron.

For a homogeneous electrolyte solution, n_m and κ do not depend on r. Then, by using Fourier transformation, one can represent Eqn (2.1) in the form

$$\tilde{\varphi}(k) = \frac{q}{2\pi^2\epsilon}\frac{1}{k^2+\kappa^2} \tag{2.4}$$

where $k = |\boldsymbol{k}|$. The inverse Fourier transformation yields

$$\varphi_m(r) = \frac{q_m}{\epsilon r}\exp(-\kappa r), \qquad r = |\boldsymbol{r}| \tag{2.5}$$

where the subscript "m" refers to the mth ion species.

The bulk density of the correlation internal energy is [31]

$$u_{cor}^{(b)} = \frac{1}{2}\lim_{r\to 0}\sum_m q_m n_m\left[\varphi_m(r) - \frac{q_m}{\epsilon r}\right] \tag{2.6}$$

Finally, from Eqns (2.2), (2.5) and (2.6) one obtains the known formula of Debye and Hückel [8]

$$u_{cor}^{(b)} = -\frac{k_B T\kappa^3}{8\pi} \tag{2.7}$$

Then the bulk density of the free energy is [8,31]

$$f_{cor}^{(b)} = T\int_T^\infty u_{cor}^{(b)}\frac{dT}{T^2} = -\frac{k_B T\kappa^3}{12\pi} \tag{2.8}$$

In the case of a plane-parallel thin liquid film $f_{cor}^{(b)} = f_{cor}^{(b)}(z)$, where the z-axis is oriented perpendicularly to the film surfaces. Our aim below is to calculate the free energy per unit area of the thin film:

$$f_{cor} = \int_0^h f_{cor}^{(b)}(z)\,dz$$

where the planes $z = 0$ and $z = h$ are the two film surfaces. The ion concentration is not constant inside the film: $n_m = n_m(z)$. However, f_{cor} is an integral quantity, which is not too sensitive to the local behavior of the functions $n_m(z)$. This fact enables one to use an appropriate model stepwise distribution for $n_m(z)$. For each step $n_m = \text{const.}$ and then the formalism for deriving Eqn (2.8) can be extended and applied. As a result one can obtain an explicit analytical expression for f_{cor}. With this end in view we consider an appropriate stepwise model of the ion distribution in the next section.

3. Stepwise model ion distribution

3.1 Single interface

Let us consider a single, plane, charged interface with surface charge density σ. The aqueous phase

is a solution of symmetrical electrolyte; the charge of a counterion is $q_1 = Ze$, whereas the charge of a co-ion is $q_2 = -Ze$ ($Z = \pm 1, \pm 2, \ldots$). Here and subsequently the indices 1 and 2 will refer to counterions and co-ions, respectively. The concentrations of both ion species are equal to n_0 far from the interface.

At given σ, Z and n_0 the classical electric double layer theory provides explicit expressions for the ion distributions $n_1(z)$ and $n_2(z)$; see Appendix A. The bulk charge density is

$$\rho(z) = Ze[n_1(z) - n_2(z)], \qquad \int_0^\infty \rho(z)\,dz = -\sigma \tag{3.1}$$

As mentioned above, for calculating the ionic-correlation energy it is convenient to replace the continuous real charge density distribution $\rho(z)$ with an idealized (model) one:

$$\rho^{id}(z) = \begin{cases} \rho^{I} & \text{for} \quad 0 < z < a \\ \rho^{II} & \text{for} \quad a < z < a_\infty \\ 0 & \text{for} \quad z > a_\infty \end{cases} \tag{3.2}$$

(see Fig. 1). Here the plane $z = 0$ represents the interface and ρ^{I}, ρ^{II}, a and a_∞ are four parameters of the model. We determine them from the following four equations, expressing conditions for equivalence between the idealized and real charge density distributions:

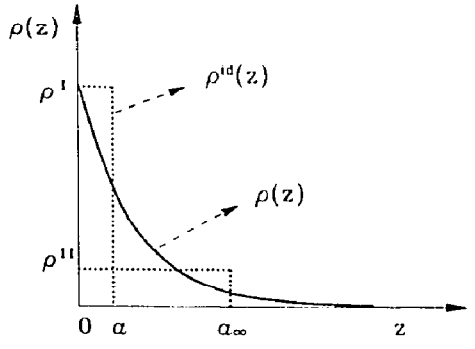

Fig. 1. Sketch of the ion-charge distribution in an electric double layer: the smooth and the stepwise profiles represent the real and model charge distributions, $\rho(z)$ and $\rho^{id}(z)$, respectively.

$$\int_0^\infty \rho^{id}(z) z^j\,dz = \int_0^\infty \rho(z) z^j\,dz \equiv Ij, \; j = 0, 1, 2 \tag{3.3}$$

$$\rho^{id}(0) = \rho(0) \tag{3.4}$$

Equations (3.3) establish equivalence between the two distributions with respect to three integral moments. Equation (3.4) calibrates the two distributions and ensures realistic description of the image forces (see below). By substituting Eqn (3.2) into Eqns (3.3) and (3.4), after some algebra, one derives explicit expressions for the parameters of the model:

$$a, a_\infty = \frac{1}{2A}[-B \pm (B^2 - 4AC)^{1/2}] \tag{3.5}$$

where a equals the smaller root, and a_∞ equals the greater root,

$$A = \sigma^2 - 2I_1\rho(0); \qquad B = 3I_2\rho(0) + 2I_1\sigma;$$
$$C = 4I_1^2 + 3I_2\sigma \tag{3.6}$$

(In view of Eqns (3.1) and (3.3), $I_0 = -\sigma$.) In addition one obtains

$$\rho^{I} = \rho(0), \qquad \rho^{II} = (2I_1 + \sigma a)/[a_\infty(a_\infty - a)] \tag{3.7}$$

The parameter a represents the width of the layer of high counterion concentration close to the interface. However, the parameter a_∞ provides a measure for the total width of the electric double layer. When two approaching double layers are separated at a distance $h < 2a_\infty$, the overlapping of the two counterion atmospheres becomes significant and noticeable repulsion between the two interfaces takes place. Values of a and a_∞ calculated for different 1:1 electrolyte concentrations are given in Table 1 (temperature 298 K, $e/\sigma = 3.5 \cdot 10^{-14}$ cm^2). One sees that both a and a_∞ decrease with increase of the electrolyte concentration.

TABLE 1

The model parameters a and a_∞, and the model Debye lengths of the double electric layer as a function of electrolyte concentration

C_{el} (M)	a (cm) ($\times 10^8$)	a_∞ (cm) ($\times 10^7$)	κ_I^{-1} (cm) ($\times 10^8$)	κ_{II}^{-1} (cm) ($\times 10^7$)	κ_0^{-1} (cm) ($\times 10^7$)
0.01	5.04	8.22	5.41	2.58	3.04
0.02	4.64	6.14	5.32	1.95	2.15
0.03	4.39	5.16	5.26	1.64	1.75
0.04	4.20	4.55	5.18	1.45	1.52
0.05	4.04	4.13	5.10	1.31	1.36

$T = 298$ K, $A = 3.5$ nm^2, 1:1 electrolyte.

Similarly to Eqn (3.2) one can write

$$n_m^{id}(z) = \begin{cases} n_m^I & \text{for} \quad 0 < z < a \\ n_m^{II} & \text{for} \quad a < z < a_\infty \\ 0 & \text{for} \quad z > a_\infty \end{cases} \tag{3.8}$$

$m = 1, 2$. We determine n_1^I and n_2^I from the equations

$$n_2^I = n_2(0), \qquad n_1^I = n_2^I + \rho^I/(Ze) \tag{3.9}$$

where $n_2(0)$ is the Poisson–Boltzmann subsurface concentration of the co-ions. The first Eqn (3.9) is a counterpart of Eqn (3.4), and the second Eqn (3.9) expresses the balance of the electrical charge.

The other two parameters, n_1^{II} and n_2^{II} we determine from the equations

$$n_2^{II} = n_2\left(\frac{a + a_\infty}{2}\right) \tag{3.10}$$

$$n_1^I = n_2^{II} + \rho^{II}/(Ze) \tag{3.11}$$

The parameters I_1, I_2, $\rho(0)$, $n_2(0)$ and $n_2[(a + a_\infty)/2]$ can be easily calculated from the Poisson–Boltzmann ion distribution as described in Appendix A.

At known ionic concentrations one can calculate the Debye parameters κ_I and κ_{II} for the respective two regions

$$\kappa_Y^2 = \frac{4\pi Z^2 e^2}{\epsilon k_B T}(n_1^Y + n_2^Y), \qquad Y = I, II \tag{3.12}$$

In Table 1 their reciprocal values are compared with a, a_∞ and with the Debye parameter

$$\kappa_0^2 = \frac{8\pi Z^2 e^2}{\epsilon k_B T} n_0 \tag{3.13}$$

for the bulk of the solution.

3.2 Thin liquid film

The overlapping of the two counterion atmospheres in the thin film changes the distribution of the ion species as compared with the case of single interface considered above. The model stepwise distribution of the charge density in a flat symmetrical film is sketched in Fig. 2.

$$\rho^{id}(z) = \begin{cases} \hat{\rho}^I & \text{for} \quad s/2 < |z| < a + s/2 \\ \hat{\rho}^{II} & \text{for} \quad |z| < s/2 \end{cases} \tag{3.14}$$

The coordinate plane $z = 0$ is placed in the middle of the film for the sake of convenience. The width of the subsurface layers is equal to a by definition. However, the electrical charge densities $\hat{\rho}^I$ and $\hat{\rho}^{II}$ in general differ from the respective densities ρ^I and ρ^{II} in the case of the single interface, compare Figs 1 and 2. The thickness of the aqueous core of the film is

$$h = s + 2a \tag{3.15}$$

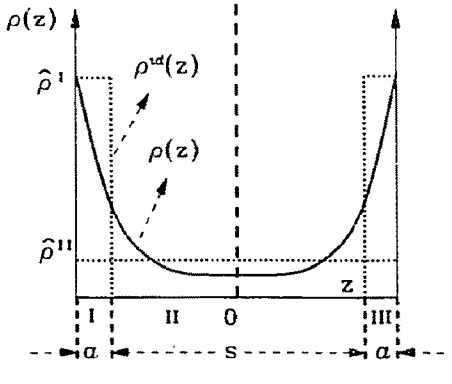

Fig. 2. Sketch of the ion-charge distribution inside a thin liquid film: the smooth and stepwise profiles represent the Poisson–Boltzmann and the idealized (model) charge density distributions, $\rho(z)$ and $\rho^{id}(z)$.

We determine $\hat{\rho}^{I}$ and $\hat{\rho}^{II}$ from the equations

$$\int_0^{h/2} \rho^{id}(z)\,dz = \int_0^{h/2} \rho(z)\,dz, \qquad \rho^{id}(h/2) = \rho(h/2) \tag{3.16}$$

which are counterparts of Eqns (3.3) and (3.4). Equation (3.16) can be transformed to read

$$a\hat{\rho}^{I} + \frac{s}{2}\hat{\rho}^{II} = -\sigma, \qquad \hat{\rho}^{I} = \rho(h/2) \tag{3.17}$$

where Eqn (3.14) and the electroneutrality condition are taken into account.

Similarly to Eqn (3.8), for the distribution of the ion species inside the thin film, one can write

$$n_m^{id}(z) = \begin{cases} \hat{n}_m^{I} & \text{for } s/2 < |z| < a + s/2 \\ \hat{n}_m^{II} & \text{for } |z| < s/2 \end{cases} \tag{3.18}$$

The model ionic concentrations $\hat{n}_m^{I}$ and $\hat{n}_m^{II}$ ($m = 1, 2$) are determined analogously to the case of a single interface:

$$\hat{n}_2^{I} = n_2(h/2), \qquad \hat{n}_1^{I} = \hat{n}_2^{I} + \hat{\rho}^{I}/(Ze) \tag{3.19}$$

$$\hat{n}_2^{II} = n_2(s/4) \tag{3.20}$$

$$\hat{n}_1^{II} = \hat{n}_2^{II} + \hat{\rho}^{II}/(Ze) \tag{3.21}$$

(Compare with Eqns (3.9)–(3.11).)

Expressions for the parameters of the Poisson–Boltzmann distribution $\rho(h/2)$, $n_2(h/2)$ and $n_2(s/4)$ are given in Appendix A.

Comparison of Figs 1 and 2 shows that the stepwise model of the ionic distribution depicted in Fig. 2 makes sense for

$$2a < h < 2a_\infty \tag{3.22}$$

However, this is just the region of physical interest. Indeed, for $h > 2a_\infty$ the overlapping of the two interfaces (and thus the film excess correlation energy) is negligible. Besides, for $h < 2a$ special effects due to the finite size of the ions become significant, see for example Refs [4,32].

The Debye parameters $\hat{\kappa}_I$ and $\hat{\kappa}_{II}$ for the respective regions inside the thin film are

$$\hat{\kappa}_Y^2 = \frac{4\pi Z^2 e^2}{\epsilon k_B T}(\hat{n}_1^Y + \hat{n}_2^Y), \qquad Y = I, II \tag{3.23}$$

4. Excess correlation energy of a thin liquid film

For an electrical charge located at $r = r_0$, Eqn (2.1) reads

$$\nabla^2\varphi - \kappa^2\varphi = -\frac{4\pi}{\epsilon} q\delta(r - r_0) \tag{4.1}$$

It is convenient to choose the coordinate system in such a way that

$$r_0 = (0, 0, \zeta) \tag{4.2}$$

where as usual the z-axis is perpendicular to the film surfaces. It is convenient to apply a two-dimensional Fourier transformation:

$$\phi(k, z) = \frac{1}{(2\pi)^2} \int_{-\infty}^{\infty}\int_{-\infty}^{\infty} dx\,dy \exp(-ik \cdot r)\varphi(r) \tag{4.3}$$

where

$$r = (x, y, z) \qquad \text{and} \qquad k = (k_x, k_y, 0) \tag{4.4}$$

In view of Eqns (4.2)–(4.4) the Fourier transform of Eqn (4.1) reads

$$\frac{\partial^2\phi}{\partial z^2} - (k^2 + \kappa^2)\phi = -\frac{q}{\pi\epsilon}\delta(z - \zeta) \tag{4.5}$$

where $k^2 = k_x^2 + k_y^2$.

The system of interest is sketched in Fig. 3. The regions I, II and III are the three homogeneous zones inside the film shown in Fig. 2. (Note that the regions I and III are similar.) The regions I–III represent the diffuse part of the electric double layer. The two narrow layers S1 and S2 represent the Stern layers at the two film surfaces. The regions IV and V are the two outer phases of the same dielectric permittivity ϵ_1 (in general $\epsilon_1 \neq \epsilon$).

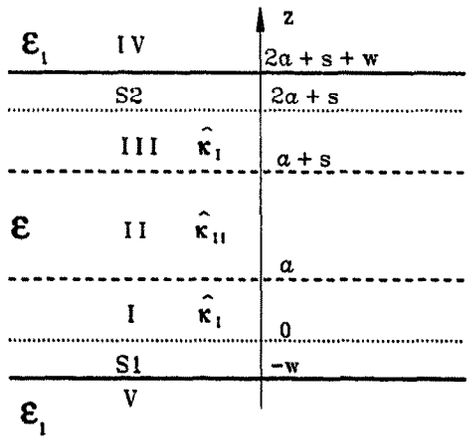

Fig. 3. Sketch of the regions of uniform ion-charge density in our model. Regions I, II, and III are the same as in Fig. 2; regions IV and V are two bulk phases adjacent to the film surfaces; regions S1 and S2 represent the two Stern layers.

4.1 Correlation energy of region I

When the point $r = r_0$ is located in region I, Eqn (4.5) reads

$$\frac{\partial^2\phi}{\partial z^2} - \lambda^2\phi = -\frac{q}{\pi\epsilon}\delta(z-\zeta) \tag{4.6}$$

where

$$\lambda^2 = k^2 + \hat{\kappa}_I^2 \tag{4.7}$$

(Compare with Eqn (3.23).) By using the variables

$$u = \lambda z; \qquad \xi = \lambda\zeta; \qquad E_1 = q/(2\pi\epsilon\lambda) \tag{4.8}$$

one transforms Eqn (4.6) to read

$$\frac{\partial^2\phi}{\partial u^2} - \phi = -2E_1\delta(u-\xi), \qquad 0 < \xi < b \tag{4.9}$$

The solution of Eqn (4.9) for region I reads [33]

$$\phi^{I}(k,u) = B_1\exp(-u) + B_2\exp u - E_1\,\mathrm{sgn}(u-\zeta)\sinh(u-\zeta),$$
$$0 < u < b \tag{4.10}$$

where B_1 and B_2 are constants, and the function $\mathrm{sgn}(x)$ is the sign of x. Note that [34]

$$\frac{\partial}{\partial x}\mathrm{sgn}(x) = 2\delta(x) \tag{4.11}$$

Since r_0 belongs to region I, the right-hand side of Eqn (4.5) is zero in region II and $\kappa = \hat{\kappa}_{II}$ in this region. Then one finds

$$\phi^{II}(k,u) = A_1\exp(-\alpha u) + A_2\exp\alpha u,$$
$$b < u < b + c \tag{4.12}$$

where A_1 and A_2 are constants and

$$\alpha^2 = (\hat{\kappa}_{II}^2 + k^2)/\lambda^2, \qquad b = \lambda a, \qquad c = \lambda s \tag{4.13}$$

Similarly one can calculate the fluctuation potentials in the remaining regions:

$$\phi^{III}(k,u) = C_1\exp(-u) + C_2\exp u,$$
$$b + c < u < 2b + c \tag{4.14}$$

$$\phi^{IV}(k,u) = D_1\exp(-\tau u), \qquad u > 2b + c + \tilde{w} \tag{4.15}$$

$$\phi^{V}(k,u) = D_2\exp(\tau u), \qquad u < -\tilde{w} \tag{4.16}$$

$$\phi^{S1}(k,u) = F_1\exp(-\tau u) + F_2\exp(\tau u),$$
$$-\tilde{w} < u < 0 \tag{4.17}$$

$$\phi^{S2}(k,u) = G_1\exp(-\tau u) + G_2\exp(\tau u),$$
$$2b + c < u < 2b + c + \tilde{w} \tag{4.18}$$

where C_i, D_i, F_i, G_i $(i = 1, 2)$ are constants,

$$\tau = k/\lambda, \qquad \tilde{w} = \lambda w \tag{4.19}$$

and w is the width of the Stern layer. The integration constants are to be determined from the standard boundary conditions

$$\phi^{Y1} = \phi^{Y2} \quad \text{and} \quad \epsilon^{Y1}\frac{\partial\phi^{Y1}}{\partial u} = \epsilon^{Y2}\frac{\partial\phi^{Y2}}{\partial u} \tag{4.20}$$

imposed at each boundary between two regions Y1 and Y2. After some tedious but simple calculations one obtains

$$\int_0^a \phi^{I}(k,\xi)\,\mathrm{d}\zeta = \lambda E_1[b/\lambda^2 + H^{I}(b,\beta,\nu)] \tag{4.21}$$

where

$$H^{I}(b,\beta,v)=\frac{a^2}{b^2P_1}\{1-\beta v+[2(\beta-1)(v-1)b-1+\beta v]\exp(-2b)\} \quad (4.22)$$

$$P_1=(1+\beta)(1+v)-(1-\beta)(1-v)\exp(-2b) \quad (4.23)$$

$$v=\alpha\frac{1-\mu}{1+\mu},\qquad \mu=\frac{1-\chi}{1+\chi}\exp(-2\alpha c),$$

$$\chi=\frac{1}{\alpha}\frac{1-\theta}{1+\theta} \quad (4.24)$$

$$\theta=\frac{1-\beta}{1+\beta}\exp(-2b),\qquad \beta=\frac{1-\eta}{1+\eta}\tau,$$

$$\eta=\frac{\epsilon-\epsilon_1}{\epsilon+\epsilon_1}\exp(-2kw) \quad (4.25)$$

The variables λ, α, b, c and τ are defined by Eqns (4.7), (4.13) and (4.19) as functions of k.

The inverse Fourier transformation of Eqn (4.21) yields

$$\int_0^a \varphi^{I}(r_2,\zeta)\,d\zeta=\frac{q}{\epsilon}\int_0^\infty dk\,kJ_0(r_2k)\times\left[\frac{a}{(k^2+\hat{\kappa}_1^2)^{1/2}}+H^{I}(b,\beta,v)\right] \quad (4.26)$$

where

$$r_2=(x,y,0),\qquad r_2=|r_2| \quad (4.27)$$

and J_0 is a Bessel function. With the help of Refs [35 and 36] one finds

$$\int_0^a \varphi^{I}(r_2,\zeta)\,d\zeta=\frac{q}{\epsilon}\left[\frac{a\exp(-\hat{\kappa}_1r_2)}{r_2}+\int_0^\infty dk\,kJ_0(r_2k)H^{I}(b,\beta,v)\right] \quad (4.28)$$

At the limit $s\to\infty$ (the upper film surface in Fig. 3 is replaced at infinity) the fluctuation potential $\varphi^{I}(r_2,\zeta)$, tends to a function $\varphi^{I}_{\infty}(r_2,\zeta)$, representing the fluctuation potential in region I of a single electric double layer, see Fig. 1. In the same limit $\hat{\kappa}_Y\to\kappa_Y$ (Y = I, II) and Eqn (4.28) transforms into

$$\int_0^a \varphi^{I}_{\infty}(r_2,\zeta)\,d\zeta=\frac{q}{\epsilon}\left[\frac{a\exp(-\kappa_1r_2)}{r_2}+\int_0^\infty dk\,kJ_0(r_2k)H^{I}(b_\infty,\beta_\infty,v_\infty)\right] \quad (4.29)$$

where

$$b_\infty=a(k^2+\kappa_1^2)^{1/2},\qquad \beta_\infty=\frac{1-\eta}{1+\eta}\frac{ka}{b_\infty}$$

and

$$v_\infty=\frac{a}{b_\infty}(k^2+\kappa_{II}^2)^{1/2} \quad (4.30)$$

are the respective limiting values of b, β and v.

The excess fluctuation potential at $r_0=(0,0,\zeta)$ due to the finite thickness of the film is

$$\Delta\varphi^{I}(\zeta)=\lim_{r_2\to0}[\varphi^{I}(r_2,\zeta)-\varphi^{I}_{\infty}(r_2,\zeta)] \quad (4.31)$$

Then from Eqns (4.28)–(4.29) and (4.31) one obtains

$$\int_0^a \Delta\varphi^{I}_m(\zeta)\,d\zeta=\frac{q_m}{\epsilon}\left\{-(\hat{\kappa}_1-\kappa_1)a+\int_0^\infty dk\times k[H^{I}(b,\beta,v)-H^{I}(b_\infty,\beta_\infty,v_\infty)]\right\} \quad (4.32)$$

where the subscript "m" refers to the mth ion species, compare with Eqn (2.5). The excess correlation internal energy per unit area of region I reads

$$\Delta u^{I}_{cor}=\int_0^a d\zeta\left[\frac{1}{2}\sum_m q_m\hat{n}^{I}_m\Delta\varphi^{I}_m(\zeta)\right] \quad (4.33)$$

(Compare with Eqns (2.6) and (4.31).) Finally, the combination of Eqns (2.3), (3.23), (4.31) and (4.33) yields

$$\Delta u^{I}_{cor} = \frac{\hat{\kappa}_I^2}{8\pi} k_B T \left\{ -(\hat{\kappa}_I - \kappa_I)a + \int_0^\infty dk\, k[H^I(b, \beta, v) - H^I(b_\infty, \beta_\infty, v_\infty)] \right\} \tag{4.34}$$

The integral in the right-hand side of Eqn (4.34) is to be solved numerically. By using the relation between internal and free energy (see Eqn (2.8)), from Eqn (4.34) one derives

$$\Delta f^{I}_{cor} = \frac{\hat{\kappa}_I^2}{8\pi} k_B T \left\{ -\frac{2}{3}(\hat{\kappa}_I - \kappa_I)a + T \int_0^\infty \frac{dT}{T^2} \int_0^\infty dk \times k[H^I(b, \beta, v) - H^I(b_\infty, \beta_\infty, v_\infty)] \right\} \tag{4.35}$$

where Δf^{I}_{cor} is the excess correlation free energy per unit area of region I. The function H^I is given by Eqns (4.22)–(4.23) above. The term proportional to $(\hat{\kappa}_I - \kappa_I)a$ accounts for the contribution of the usual Debye–Hückel screening in a homogeneous solution, whereas the integral term in Eqn (4.35) accounts for both the image forces and solution inhomogeneity (see also the discussion in Section 4.3 below). It is worthwhile noting that H^I depends on T through κ_I and $\hat{\kappa}_I$, see Eqns (3.12) and (3.23), where the concentrations n^I_m and $\hat{n}^I_m$ $(m = 1, 2)$ must be kept constant during the integration with respect to T.

4.2 Correlation energy of region II

In this case $b < \xi < b + c$. Instead of Eqns (4.10) and (4.12) one has

$$\phi^I(k, u) = B_1 \exp(-u) + B_2 \exp(u), \qquad 0 < u < b \tag{4.36}$$

$$\phi^{II}(k, u) = A_1 \exp(-\alpha u) + A_2 \exp(\alpha u) - E_2 \operatorname{sgn}(u - \zeta) \sinh \alpha(u - \xi), \qquad b < u < b + c \tag{4.37}$$

where

$$E_2 = E_1/\alpha$$

Equations (4.14)–(4.18) also hold in the present case. The integration constants A_i, B_i, C_i, D_i, F_i and G_i $(i = 1, 2)$ can be determined from the boundary conditions (Eqn (4.20)). The result of these simple but tedious calculations reads

$$\int_a^{a+s} \phi^{II}(k, \xi)\, d\zeta = \alpha\lambda E_2 [c/(\alpha\lambda)^2 + H^{II}(c, \alpha, \chi)] \tag{4.38}$$

where

$$H^{II}(c, \alpha, \chi) = \frac{s^2}{c^2 P_2}\{1 - \chi^2 + [2\alpha c(1 - \chi)^2 - 1 + \chi^2] \times \exp(-2\alpha c)\} \tag{4.39}$$

$$P_2 = \alpha^2[(1 + \chi)^2 - (1 - \chi)^2 \exp(-2\alpha c)] \tag{4.40}$$

and the variables λ, α, c and χ are defined by Eqns (4.7), (4.13) and (4.24). By using the inverse Fourier transformation one derives a counterpart of Eqn (4.28) for region II:

$$\int_a^{a+s} \varphi^{II}(r_2, \zeta)\, d\zeta = \frac{q}{\epsilon}\left[\frac{s \exp(-\hat{\kappa}_{II} r_2)}{r_2} + \int_0^\infty dk\, k J_0(r_2 k) H^{II}(c, \alpha, \chi) \right] \tag{4.41}$$

At the limit $s \to \infty$ the fluctuation potential $\varphi^{II}(r_2, \zeta)$ tends to a function $\varphi^{II}_\infty(r_2, \zeta)$, representing the fluctuation potential in region II of a single electric double layer, see Fig. 1. In the same limit, $\hat{\kappa}_Y = \kappa_Y$ (Y = I, II). Then the integral over

$\varphi^{II}_{\infty}(r_2, \zeta)$ reads

$$\int_a^{a+s} \varphi^{II}_{\infty}(r_2, \zeta)\, d\zeta = \frac{q}{\epsilon}\left[\frac{s \exp(-\kappa_{II} r_2)}{r_2} + \int_0^{\infty} dk\, k J_0(r_2 k) H^{II}(c_{\infty}, \alpha_{\infty}, \chi_{\infty})\right] \tag{4.42}$$

where

$$c_{\infty} = s\sqrt{k^2 + \kappa_I^2}, \qquad \alpha_{\infty} = (s/c_{\infty})\sqrt{k^2 + \kappa_{II}^2},$$

$$\chi_{\infty} = \frac{1}{\alpha_{\infty}} \frac{1 - \theta_{\infty}}{1 + \theta_{\infty}} \tag{4.43}$$

$$\theta_{\infty} = \frac{1 - \beta_{\infty}}{1 + \beta_{\infty}} \exp(-2b_{\infty}) \tag{4.44}$$

b_{∞} and β_{∞} are given by Eqn (4.30). Similarly to Eqn (4.31) one can define the excess fluctuation potential at the point $r_0 = (0, 0, \zeta)$ in region II:

$$\Delta\varphi^{II}(\zeta) = \lim_{r_2 \to 0} [\varphi^{II}(r_2, \zeta) - \varphi^{II}_{\infty}(r_2, \zeta)] \tag{4.45}$$

Then analogously to Eqn (4.34), by integrating $\Delta\varphi^{II}(\zeta)$ one obtains the excess correlation internal and free energies per unit area of region II:

$$\Delta u^{II}_{cor} = \frac{\hat{\kappa}_{II}^2}{8\pi} k_B T \left\{-(\hat{\kappa}_{II} - \kappa_{II})s + \int_0^{\infty} dk\, k[H^{II}(c, \alpha, \chi) - H^{II}(c_{\infty}, \alpha_{\infty}, \chi_{\infty})]\right\} \tag{4.46}$$

$$\Delta f^{II}_{cor} = \frac{\hat{\kappa}_{II}^2}{8\pi} k_B T \left\{-\frac{2}{3}(\hat{\kappa}_{II} - \kappa_{II})s + T \int_T^{\infty} \frac{dT}{T^2} \int_0^{\infty} dk \times k[H^{II}(c, \alpha, \chi) - H^{II}(c_{\infty}, \alpha_{\infty}, \chi_{\infty})]\right\} \tag{4.47}$$

The function H^{II} is defined by Eqns (4.39)–(4.40).

Since region III is similar to region I (see Figs 2 and 3), the total excess internal and free energies per unit area of the film are:

$$\Delta u_{cor} = 2\Delta u^{I}_{cor} + \Delta u^{II}_{cor}, \qquad \Delta f_{cor} = 2\Delta f^{I}_{cor} + \Delta f^{II}_{cor} \tag{4.48}$$

The derivative of Δf_{cor} with respect to the film thickness equals the ionic-correlation component of the disjoining pressure:

$$\Pi_{cor} = -[\partial(\Delta f_{cor})/\partial h]_T \tag{4.49}$$

The numerical data (see Section 5 below) show that both Δf_{cor} and Π_{cor} have negative sign, i.e. they correspond to attraction between the film surfaces. Hence Δf_{cor} and Π_{cor} are to be compared with the respective contributions of the van der Waals attractive forces [5,37]:

$$\Delta f_{vw} = -\frac{A_H}{12\pi h_w^2}, \qquad \Pi_{vw} = -\frac{A_H}{6\pi h_w^3} \tag{4.50}$$

h_w is the equivalent water thickness of the film accounting not only for the diffuse double layer but also for the two Stern layers and the two surface monolayers, see for example Ref. [38]. A comparison shows that the ion-correlation effect often exceeds in magnitude the effect of conventional van der Waals forces (Section 5 below).

4.3 Effect of the image forces

The contribution of the image forces is automatically incorporated in Eqns (4.35) and (4.47). To visualize this consider the case when there is no Stern layer: $w = 0$. If such is the case, from Eqn (4.25) one obtains

$$\eta|_{w=0} = \Delta_1, \qquad \Delta_1 = \frac{\epsilon - \epsilon_1}{\epsilon + \epsilon_1} \tag{4.51}$$

Then Eqns (4.28)–(4.29) can be represented in the form

$$\int_0^{a} \varphi^{I}(r_2, \zeta)\, d\zeta = \frac{q}{\epsilon}\left[\frac{a \exp(-\hat{\kappa}_I r_2)}{r_2} + \frac{\Delta_1}{2} K_0(\hat{\kappa}_I r_2)\right.$$

$$+\int_0^\infty \mathrm{d}k\, kJ_0(r_2k)L^{\mathrm{I}}(b,\beta,v)\Bigg] \qquad (4.52)$$

(4.48)

$$\int_0^a \varphi^{\mathrm{I}}_\infty(r_2,\zeta)\,\mathrm{d}\zeta = \frac{q}{\epsilon}\Bigg[\frac{a\exp(-\kappa_{\mathrm{I}}r_2)}{r_2}+\frac{\Delta_1}{2}K_0(\kappa_{\mathrm{I}}r_2)$$

$$+\int_0^\infty \mathrm{d}k\, kJ_0(r_2k)L^{\mathrm{I}}(b_\infty,\beta_\infty,v_\infty)\Bigg] \qquad (4.53)$$

where the integral terms are regular at $r_2 \to 0$;

$$L^{\mathrm{I}}(b,\beta,v) = \frac{a^2}{b^2}\Bigg\{\frac{1-\beta v}{P_1}-\frac{\Delta_1}{2} + [2b(\beta-1)(v-1)-1+\beta v] \times \exp(-2b)/P_1\Bigg\} \qquad (4.54)$$

where P_1 is given by Eqn (4.23). K_0 is a modified Bessel function which is logarithmically divergent at $r_2 \to 0$. Nevertheless, the excess fluctuation potential, $\Delta\varphi^{\mathrm{I}}(\zeta)$, turns out to be finite (see Eqn (4.31)) and the expression for $\Delta f^{\mathrm{I}}_{\mathrm{cor}}$, Eqn (4.35), is also regular:

$$\Delta f^{\mathrm{I}}_{\mathrm{cor}} = \frac{\hat{\kappa}_{\mathrm{I}}^2}{8\pi}k_{\mathrm{B}}T\Bigg\{-\frac{2}{3}(\hat{\kappa}_{\mathrm{I}}-\kappa_{\mathrm{I}})a-\frac{\Delta_1}{2} \times \ln(\hat{\kappa}_{\mathrm{I}}/\kappa_{\mathrm{I}}) + T\int_T^\infty \frac{\mathrm{d}T}{T^2}\int_0^\infty \mathrm{d}k \times k[L^{\mathrm{I}}(b,\beta,v)-L^{\mathrm{I}}(b_\infty,\beta_\infty,v_\infty)]\Bigg\}$$

for $w=0$ (4.55)

One can prove that the terms in Eqns (4.52), which are divergent proportionally to $(1/r_2)$ and $\ln(r_2)$, are due to the electric charge at the point $(0, 0, \zeta)$ and its image at the point $(0, 0, -\zeta)$, respectively. Then the first and second terms in the braces in Eqn (4.55) can be attributed to the Debye screening and to the image forces, respectively. For a film formed from an aqueous solution between two air or oil phases $\Delta_1 > 0$ and $\hat{\kappa}_{\mathrm{I}} > \kappa_{\mathrm{I}}$. Then the logarithmic term in Eqn (4.55) gives a negative contribution to $\Delta f^{\mathrm{I}}_{\mathrm{cor}}$. In other words, the image forces lead to an effective attraction between the film surfaces. However, this is not the case for films between conductors, as shown below.

4.4 Film between two electro-conductive phases

When phases IV and V (see Fig. 3) are conductors of electricity, the boundary conditions at the film surfaces are

$$\phi^{\mathrm{I}}|_{u=0} = \phi^{\mathrm{III}}|_{u=\lambda h} = 0 \qquad (4.56)$$

i.e. one is dealing with a Dirichlet boundary problem. Δf_{cor} can be found in the same way as for a film between dielectrics. That is why we skip the details and give the final expressions for $\Delta f^{\mathrm{I}}_{\mathrm{cor}}$ and $\Delta f^{\mathrm{II}}_{\mathrm{cor}}$ in the case $w=0$ (negligible Stern layer):

$$\Delta f^{\mathrm{I}}_{\mathrm{cor}} = \frac{\hat{\kappa}_{\mathrm{I}}^2}{8\pi}k_{\mathrm{B}}T\Bigg\{-\frac{2}{3}(\hat{\kappa}_{\mathrm{I}}-\kappa_{\mathrm{I}})a+\frac{1}{2} \times \ln(\hat{\kappa}_{\mathrm{I}}/\kappa_{\mathrm{I}}) + T\int_T^\infty \frac{\mathrm{d}T}{T^2}\int_0^\infty \mathrm{d}k \times k[D^{\mathrm{I}}(b,\alpha,k)-D^{\mathrm{I}}(b_\infty,\alpha_\infty,k)-G^{\mathrm{I}}(k)]\Bigg\} \qquad (4.57)$$

$$\Delta f^{\mathrm{II}}_{\mathrm{cor}} = \frac{\hat{\kappa}_{\mathrm{II}}^2}{8\pi}k_{\mathrm{B}}T\Bigg\{-\frac{2}{3}(\hat{\kappa}_{\mathrm{II}}-\kappa_{\mathrm{II}})s + T\int_T^\infty \frac{\mathrm{d}T}{T^2}\int_0^\infty \mathrm{d}k \times k[D^{\mathrm{II}}(b,\alpha,k)-D^{\mathrm{II}}_\infty(b_\infty,\alpha_\infty,k)-G^{\mathrm{II}}(k)]\Bigg\} \qquad (4.58)$$

where

$$D^{\mathrm{I}}(b,\alpha,k) = \frac{a^2}{b^2Q_1}\{1-\alpha+[1+\alpha-4b(1-\alpha)] \times \exp(-2b)\} \qquad (4.59)$$

$$Q_1 = 2[1 + \alpha + (1 - \alpha)\exp(-2b)] \tag{4.60}$$

$$G^{I}(k) = 2\alpha l[\tanh b - b/\cosh^2 b]a^2/(b^2 Q_2) \tag{4.61}$$

$$Q_2 = (1 + \alpha \tanh b)^2 - (1 - \alpha^2 \tanh^2 b)l \tag{4.62}$$

$$l = \Lambda(b, \alpha)\exp(-2\alpha c), \qquad \Lambda(b, \alpha) = \frac{1 - \alpha \tanh b}{1 + \alpha \tanh b} \tag{4.63}$$

$$D^{II}(b, \alpha, k) = [1 - \exp(-s\sqrt{k^2 + \hat{\kappa}_{II}^2})] \times \Lambda(b, \alpha)/(k^2 + \hat{\kappa}_{II}^2) \tag{4.64}$$

$$D_{\infty}^{II}(b_{\infty}, \alpha_{\infty}, k) = [1 - \exp(-s\sqrt{k^2 + \kappa_{II}^2})] \times \Lambda(b_{\infty}, \alpha_{\infty})/(k^2 + \kappa_{II}^2) \tag{4.65}$$

$$G^{II}(k) = \frac{1}{1 + g}\left[\frac{\Lambda(b, \alpha)}{\alpha^2 \lambda^2}[1 - \exp(-\alpha c)] \times [\exp(-\alpha c) + g] - 2sg/(\lambda\alpha)\right] \tag{4.66}$$

$$g = \Lambda^2(b, \alpha)\exp(-2\alpha c) \tag{4.67}$$

The total excess correlation energy is given again by Eqn (4.48). It is worthwhile noting that the term proportional to $\ln(\hat{\kappa}_1/\kappa_1)$ in Eqn (4.57) gives a positive contribution to Δf_{cor}. Hence in the case under consideration the image forces give rise to effective repulsion between the film surfaces. In spite of that Δf_{cor} is still negative, but smaller in magnitude compared with the case of film between dielectrics (see Fig. 9 below).

5. Numerical data and discussion

The equations derived in the previous section enable us to study the role of different factors on the correlation excess free energy of the film, Δf_{cor}. The latter is to be compared with the excess free energies Δf_{el} and Δf_{vw}, which are due to the electrostatic and van der Waals interactions, respectively. The total excess free energy Δf per unit area of the film is

$$\Delta f = \Delta f_{el} + \Delta f_{vw} + \Delta f_{cor} \tag{5.1}$$

Δf is simply connected with the contact angle θ, which is an experimentally measurable parameter [28,39,40]:

$$\cos\theta = 1 + \Delta f/(2\sigma) \tag{5.2}$$

where σ is the solution surface tension. The disjoining pressure

$$\Pi = -\left(\frac{\partial \Delta f}{\partial h}\right)_T \tag{5.3}$$

is another quantity given by experiment, see for example Refs [5,27 and 28]. Similarly to Eqn (5.1) one can write

$$\Pi = \Pi_{el} + \Pi_{vw} + \Pi_{cor} \tag{5.4}$$

where Π_{el}, Π_{vw} and Π_{cor} are the electrostatic and van der Waals and correlation components of disjoining pressure; compare with Eqn (4.49).

To calculate Δf_{el} in Eqn (5.1) we used the rigorous formula of Muller; see Eqn (A27) in Appendix A. Δf_{cor} was calculated by means of Eqn (4.48) along with Eqns (4.22)–(4.25), (4.30), (4.35), (4.39)–(4.40), (4.43)–(4.44) and (4.47); see Appendix B for the algorithm of calculation. Δf_{vw} was calculated by means of Eqn (4.50), where we used the expression

$$h_w = h + \Delta h \tag{5.5}$$

where, as usual in this paper, h is the thickness of the diffuse electric double layer inside the film, whereas Δh accounts for the two surface layers. For foam films stabilized with ionic surfactants, Δh is very close to the equivalent water thickness of the ultrathin Newton black films consisting practically of two surfactant monolayers [28,39]. That is why in our numerical calculations we use $\Delta h = 4$ nm, which is a quantity of the order of the thickness of such ultrathin films.

In Fig. 4 the sum $\Pi_{el} + \Pi_{cor}$ is plotted as a function of h, calculated by means of our model (the solid curve), and compared with results of other authors for electrolyte concentration $C_{el} = 0.002$ mol l^{-1} and area per unit surface charge $A = 0.6$ nm^2. (By unit charge here and subsequently we understand the charge of the electron.) The

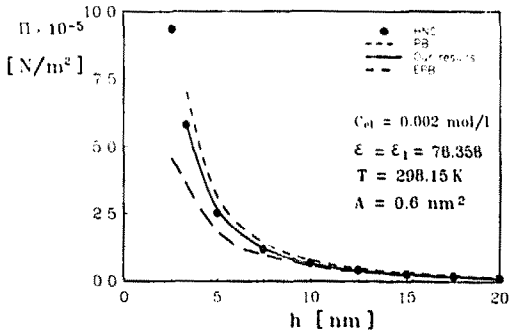

Fig. 4. Plot of $(\Pi_{el} + \Pi_{cor})$ vs film thickness h at 0.002 mol l^{-1} 1:1 electrolyte concentration. Short dashed curve, $\Pi_{cor} = 0$; solid curve, our model; long dashed curve, EPB theory [26]; the points (●) represent numerical results of HNC-closure.

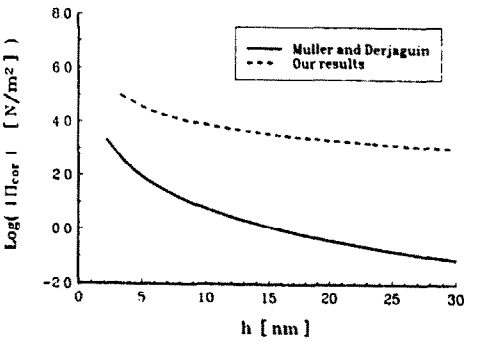

Fig. 5. Plot of Π_{cor} vs h calculated by means of our approach (dashed curve) and by the theory of Muller and Derjaguin [5,15] at $C_{el} = 0.01$ mol l^{-1} concentration of 1:1 electrolyte and area per unit surface charge $A = 3.5$ nm^2.

algorithm of our calculations is described in Appendix B. In particular, Π_{el} is calculated by means of Eqn (A28)—see the short-dashed curve in Fig. 4. The long-dashed curve represents $\Pi_{el} + \Pi_{cor}$ calculated by means of the EPB theory of Attard et al. [26]. The points represent numerical data of Kjellander and Marčelja obtained by means of HNC-closure; see Fig. 3 in Ref. [26]. A good agreement between our model and the HNC data is observed. This result confirms our suggestion that the real smooth ionic charge distribution can be replaced by a model stepwise distribution without decreasing the accuracy of calculation of integral quantities like Δf_{cor} and Π_{cor}.

This conclusion is confirmed by the comparison with other numerical data given in Ref. [26]. Namely, for concentration $C_{el} = 0.1$ mol l^{-1}, 1:1 electrolyte, $A = 5$ nm^2 and $h = 5$ nm, the calculated values of $\Pi_{el} + \Pi_{cor}$ are the following: $0.96 \cdot 10^4$ N m^{-2} from HNC, $1.09 \cdot 10^4$ N m^{-2} from EPB and $1.01 \cdot 10^4$ N m^{-2} from our theory. The difference between HNC and our theory is probably due to the effect of the finite ion size, which is not taken into account either in our theory, or in EPB. For comparison $\Pi_{el} = 1.20 \cdot 10^4$ N m^{-2}.

We also compared our approach with the theory of Muller and Derjaguin [5,15]; see Fig. 5. The pronounced difference between the results of these two theories is probably due to the very simplified model used by Muller and Derjaguin.

To study the effect of the outer-phase dielectric permittivity, ϵ_1, on Δf_{cor}, we varied ϵ_1 between 0 and 78.4. As seen in Fig. 6 this variation does not result in a considerable effect on Δf_{cor}. In particular, the curves with $\epsilon_1 = 0$ and $\epsilon_1 = 1$ practically coincide. Hence for foam films ($\epsilon_1 = 1$) one can use the Neumann boundary condition ($\epsilon_1 = 0$, $\epsilon \neq 0$); compare with Eqn (4.20).

The effect of the width, w, of the Stern layers at the two film surfaces, is examined in Fig. 7. Δf_{cor} is calculated for two different values of w: $w = 0$ and $w = 0.3$ nm. The curve with $w = 0.6$ nm is very close to that corresponding to $w = 0.3$ nm and cannot be visualized in Fig. 7. In general, the effect of Stern layer thickness w is more pronounced than the effect of the outer-phase dielectric permittivity; compare Figs 6 and 7. It is worthwhile noting that the excess free energy Δf_{cor} is finite at the limit $w \to 0$. This is due to the exact cancellation

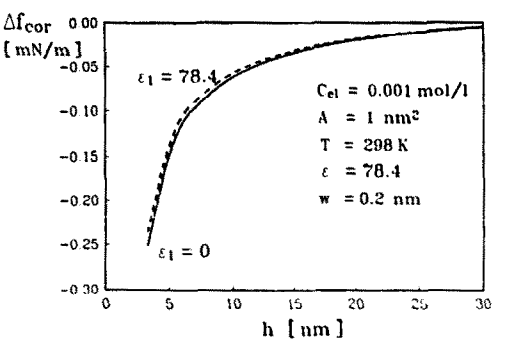

Fig. 6. Excess correlation free energy Δf_{cor} vs film thickness h at different dielectric permittivities of the outer phase, ϵ_1.

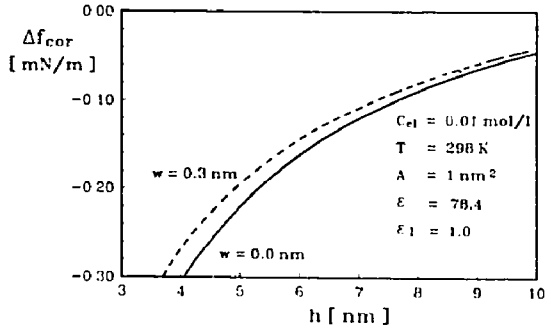

Fig. 7. Excess correlation free energy Δf_{cor} vs film thickness h at different widths of the Stern layer, w.

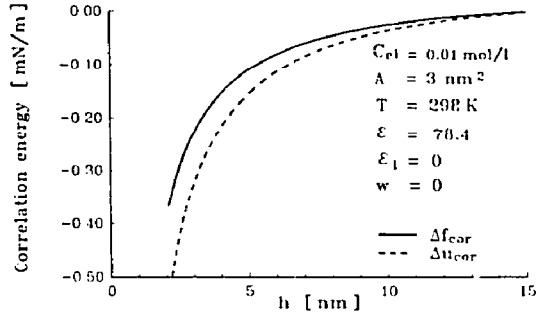

Fig. 8. Isotherms of the correlation excess free energy, Δf_{cor}, and internal energy Δu_{cor}, per unit area of a thin film vs the film thickness h.

of the two logarithmic divergencies due to the image forces; see Section 4.3 above.

The plots of the free correlation energy Δf_{cor} and of the internal correlation energy Δu_{cor} vs film thickness h are compared in Fig. 8. One sees that under the same conditions Δu_{cor} is systematically larger in magnitude than Δf_{cor}.

Figure 9 shows that the magnitude of Δf_{cor} is markedly larger in the case of gaseous outer phases (the Neumann boundary problem: $d\varphi/dz = 0$ at the boundaries) compared with the case of metal outer phases (the Dirichlet boundary problem: $\varphi = 0$ at the boundaries). This result is connected with the fact that the contribution of the image forces has opposite signs for the Dirichlet and Neumann problems; see Section 4.2 above.

According to Eqn (5.1) the total excess free energy per unit area of the thin film, Δf, is a superposition of the contributions due to the electrostatic, van der Waals and ionic-correlation

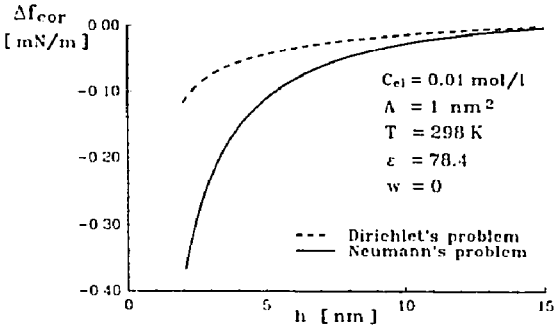

Fig. 9. Correlation excess free energy Δf_{cor} vs the film thickness h for two different boundary conditions: Dirichlet problem (film between two electroconducting phases) and Neumann problem (film between two gaseous phases).

interactions. The different components of Δf are compared in Fig. 10 for the case of $C_{el} = 0.01$ mol l^{-1} 1:1 electrolyte concentration, area per unit surface charge $A = 1$ nm^2, $T = 298$ K, $\epsilon = 78.4$, $\epsilon_1 = 1$, $w = 0.2$ nm. Δf_{vw} and Δf_{el} are calculated from Eqns (4.50) and (A27). Here and subsequently for calculating Δf_{vw} and Π_{vw} we use the Hamaker constant $A_H = 4.5 \cdot 10^{-13}$ erg and $\Delta h = 4$ nm, which are typical values for foam films. (For emulsion films A_H, and hence Δf_{vw} and Π_{vw}, is less by one order of magnitude.) One sees in Fig. 10 that $|\Delta f_{cor}|$ turns out to be considerably larger than $|\Delta f_{vw}|$, both of them corresponding to attraction between the film surfaces. In spite of that, the electrostatic repulsion is strong enough to determine the positive sign of Δf in the range of film thicknesses considered.

In Fig. 11 the role of the electrolyte concen-

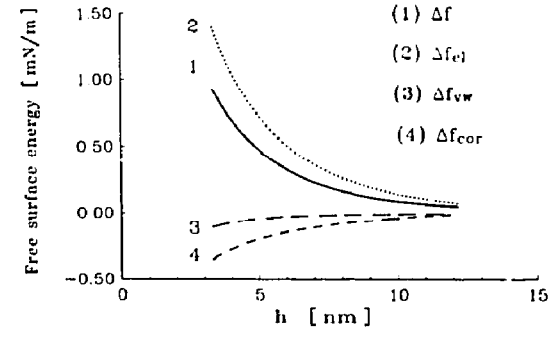

Fig. 10. The total excess free energy Δf and its electrostatic (Δf_{el}), van der Waals (Δf_{vw}) and ionic-correlation (Δf_{cor}) components vs the film thickness h.

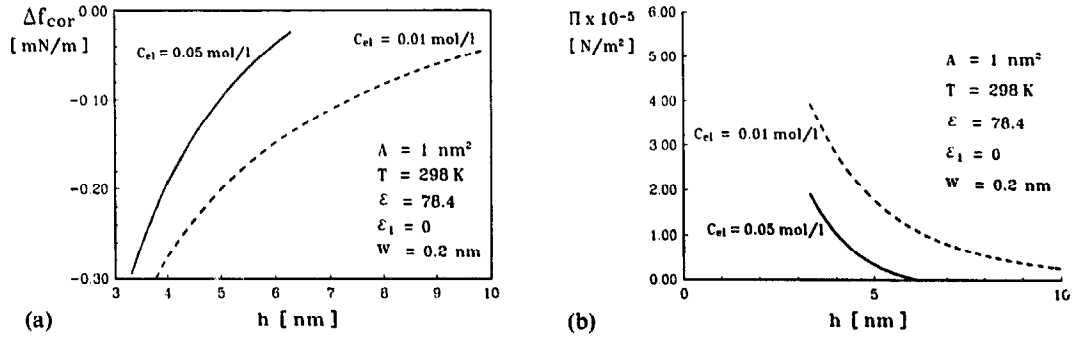

Fig. 11. Dependence of (a) the excess correlation free energy Δf_{cor} and (b) the total disjoining pressure Π on the film thickness h at different electrolyte concentrations, C_{el}.

tration in the bulk solution, C_{el}, is examined. Figure 11(a) shows that the magnitude of the correlation excess free energy Δf_{cor} is larger for the lower electrolyte concentration. However, the same is true for the electrostatic free energy Δf_{el}. Since for a 1:1 electrolyte Δf_{el} exceeds $|\Delta f_{cor}|$, the total excess free energy Δf and the disjoining pressure correspond to repulsion (Fig. 11(b)).

The situation changes considerably for a 2:2 electrolyte. As shown in Fig. 12(a), $|\Pi_{cor}|$ is larger for a 2:2 electrolyte than for a 1:1 electrolyte at the same bulk concentration, C_{el}. Moreover, the total disjoining pressure Π turns out to be negative for a 2:2 electrolyte, whereas it is positive for a 1:1 electrolyte; see Fig. 12(b). Negative values of Π have been also obtained by other authors [21] with 2:2 electrolytes.

Figures 13(a)–13(b) illustrate how the magnitude of the surface charge density, $|\sigma|$, affects the excess free energy. As earlier, we use the area per unit surface charge, $A = e/|\sigma|$, as a measure for the surface charge. One sees that in Fig. 13(a) the greater the surface charge density (the smaller A), the greater the magnitude of the attractive correlation free energy Δf_{cor}. However, the repulsive electrostatic energy Δf_{el} strongly increases with the increase of the surface charge. So, it turns out that the total free energy Δf is repulsive and increases with the increase of the surface charge density at the same bulk concentration $C_{el} = 0.01$ mol l^{-1} of a 1:1 electrolyte; see Fig. 13(b).

The temperature enters the expression for the ionic-correlation free energy Δf_{cor}, both explicitly and implicitly, through the dielectric permittivity of the medium ϵ. Figure 14 represents the plot of Δf_{cor} vs h for two different temperatures. The respective experimental values of ϵ are taken from Ref. [41]. One sees that, in spite of the comparatively great temperature interval (40 K), the change in Δf_{cor} is not too large. At the end of this section

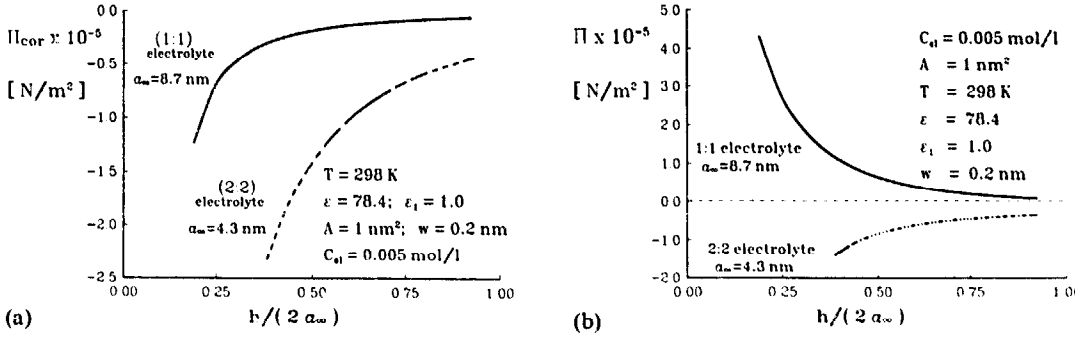

Fig. 12. Plots of (a) the ionic-correlation and (b) the total disjoining pressures, Π_{cor} and Π vs the film thickness h for 1:1 and 2:2 electrolytes at the same electrolyte concentration.

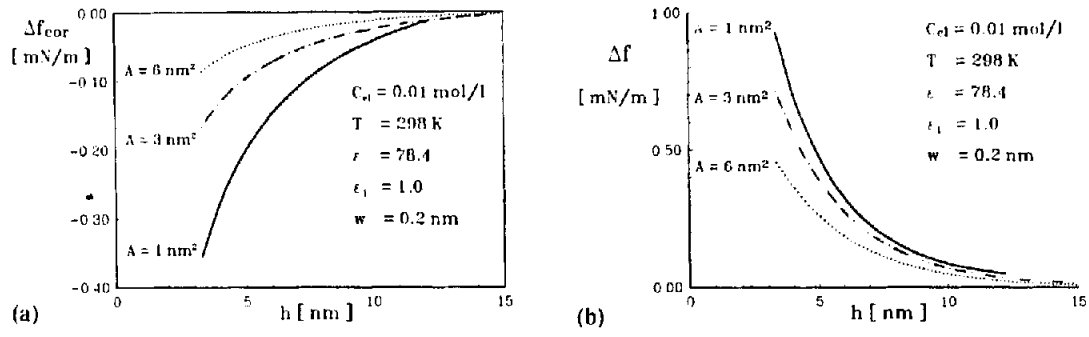

Fig. 13. Plots of (a) the ionic correlation and (b) the total excess free energies, Δf_{cor} and Δf, vs the film thickness h at different values of the area per unit surface charge, A.

we recall that the algorithm for calculating the excess free energy Δf and disjoining pressure Π is given in Appendix B.

6. Concluding remarks

Our aim in the present study is to calculate the contribution Δf_{cor} of the ionic correlations to the excess free energy per unit area of thin liquid films formed from electrolyte solutions. From the expression for Δf_{cor} one can easily calculate the ionic-correlation contributions to the disjoining pressure and contact angle; see Eqns (4.49) and (5.1)–(5.2). Δf_{cor} accounts for the following effects:

(i) energy of formation of Debye counterion atmosphere around each ion in the film;

(ii) energy of deformation of the counterion atmosphere due to the image forces, i.e. to the fact that unlike a bulk solution, the film interior is not an isotropic uniform phase;

(iii) energy of the long-range correlations between charge density fluctuations in the two opposite electric double layers.

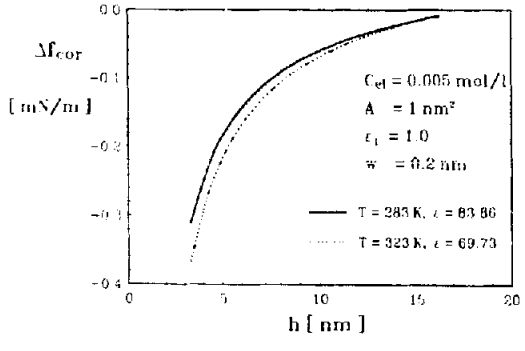

Fig. 14. Plot of the ionic-correlation free energy Δf_{cor} vs the film thickness h at two different temperatures.

The above three effects can be related to the three terms in the right-hand side of Eqn (4.55).

The method we used to calculate Δf_{cor} is an extension of the Debye–Hückel method based on Eqn (2.1). Utilizing the fact that Δf_{cor} represents the integral of the bulk density of the correlation free energy along the transversal to the film surfaces, we used a stepwise model ion-charge distribution inside the film; see Fig. 2. The stepwise model profile is equivalent to the continuous Poisson–Boltzmann charge density distribution with respect to several integral characteristics (Eqn (3.3)). By solving Eqn (2.1) for each uniform region of the model charge density profile, along with appropriate boundary conditions, we arrived at comparatively simple expressions for the excess correlation internal and free energies Δu_{cor} and Δf_{cor}; see Eqns (4.34)–(4.35) and (4.46)–(4.48). Numerically these expressions turn out to be closer to the HNC-data of Kjellander and Marčelja than to the EPB theory of Attard et al. [26], who have used the continuous Poisson–Boltzmann charge distribution at the cost of much more complicated mathematics; cf. Fig. 4.

The expressions derived were then applied to examine the effect of different factors on Δf_{cor} and Π_{cor}. The main conclusions are the following.

(1) When the two outer phases are dielectrics of permittivity ϵ_1, the variation of ϵ_1 between 0 and 80 does not affect Δf_{cor} significantly; see Fig. 6.

(2) When the outer phases are metals or conductors, Δf_{cor} is considerably smaller than in the case of dielectrics; see Fig. 9.

(3) The increase of the width, w, of the Stern layer between 0 and 3 Å can change Δf_{cor} up to 5–10%; see Fig. 7. Further increase of w does not cause appreciable changes in Δf_{cor}.

(4) In all cases examined Δf_{cor} is negative and corresponds to attraction, which in many cases exceeds the van der Waals attraction; see Fig. 10.

(5) The increase of electrolyte concentration decreases the magnitude of Δf_{cor} (Fig. 11(a)).

(6) In the case of a 2:2 electrolyte the attractive forces can prevail and the total free energy Δf and disjoining pressure can be negative (Fig. 12).

(7) The increase of surface charge density increases the magnitude of Δf_{cor} (Fig. 13).

(8) The increase of temperature leads to a slight increase of $|\Delta f_{cor}|$, (Fig. 14).

It should be noted that all these conclusions are valid for film thicknesses much greater than the ion diameter, because we used the concept for point ions.

In conclusion, the effect of ionic correlations yields an important contribution to the balance of different surface forces in thin liquid films. This effect gives rise to an attractive force, which can be comparable with, or even considerably greater than, the van der Waals attraction.

Acknowledgment

This work was financially supported by the Bulgarian Ministry of Science and Higher Education.

References

1 B.V. Derjaguin and L.D. Landau, Acta Physicochim. USSR, 14 (1941) 633.
2 E.J.W. Verwey and J.Th. Overbeek, The Theory of Stability of Lyophobic Colloids. Elsevier, Amsterdam, 1948.
3 H. Sontag and K. Strange, Coagulation and Stability of Disperse Systems, Halsted Press, New York, 1972.
4 M.J. Grimson, P. Richmond and C.S. Vassilieff, in I.B. Ivanov (Ed.), Thin Liquid Films, Marcel Dekker, New York, 1988, p. 275.
5 B.V. Derjaguin, Theory of Stability of Colloids and Thin Films, Nauka, Moscow, 1986 (in Russian); Plenum Press, New York, 1989.
6 J.Th.G. Overbeek, in H.R. Kryit (Ed.), Colloid Science, Vol. 1, Elsevier, Amsterdam, 1952, Chapter 8.
7 R.J. Hunter, Zeta Potential in Colloid Science, Academic Press, New York, 1981, pp. 241–242.
8 P. Debye and E. Hückel, Phys. Z., 24 (1923) 185.
9 G.A. Martynov, in B.V. Derjaguin (Ed.), Research in Surface Forces, Vol. 2, Consultants Bureau, New York, 1966.
10 C.W. Outhwaite, J. Chem. Soc., Faraday Trans. 2, 74 (1978) 1214.
11 S. Levine and C.W. Outhwaite, J. Chem. Soc., Faraday Trans. 2, 74 (1978) 1670.
12 C.W. Outhwaite, L.B. Bruiyan and S. Levin, J. Chem. Soc., Faraday Trans. 2, 76 (1980) 1338.
13 G.M. Torrie and J.P. Valleau, J. Chem. Phys., 73 (1980) 5807.
14 G.M. Torrie, J.P. Valleau and G.N. Patey, J. Chem. Phys., 76 (1982) 4615.
15 V.M. Muller and B.V. Derjaguin, Colloids Surfaces, 6 (1983) 205.
16 V.N. Gorelkin and V.P. Smilga, Sov. Phys. JETP, 36 (1973) 761.
17 D.J. Mitchell and P. Richmond, J. Colloid Interface Sci., 46 (1974) 118.
18 P. Richmond, J. Chem. Soc., Faraday Trans. 2, 70 (1974) 1066.
19 P. Richmond, J. Chem. Soc., Faraday Trans. 2, 70 (1974) 1650.
20 S.L. Carnie and D.Y.C. Chan, Mol. Phys., 51 (1984) 1047.
21 L. Guldbrand, B. Jönsson, H. Wennerström and P. Linse, J. Chem. Phys., 80 (1984) 2221.
22 R. Kjellander and S. Marčelja, J. Chem. Phys., 82 (1985) 2122.
23 R. Kjellander and S. Marčelja, Chem. Phys. Lett., 112 (1984) 49.
24 R. Kjellander and S. Marčelja, J. Chem. Phys., 90 (1986) 1230.
25 P. Attard, D.J. Mitchell and B.W. Ninham, J. Chem. Phys., 88 (1988) 4987.
26 P. Attard, D.J. Mitchell and B.W. Ninham, J. Chem. Phys., 89 (1988) 4358.
27 D. Exerowa, T. Kolarov and Khr. Khristov, Colloids Surfaces, 22 (1987) 171.
28 P.M. Kruglyakov, in I.B. Ivanov (Ed.), Thin Liquid Films, Marcel Dekker, New York, 1988, p. 767.
29 V.N. Paunov and P.A. Kralchevsky, Colloids Surfaces, 64 (1992) 265.
30 E.M. Lifshitz and L.P. Pitaevsky, Theoretical Physics, Vol. 9, Statistical Physics 2, Nauka, Moscow, 1978 (in Russian).
31 L.D. Landau and E.M. Lifshitz, Statistical Physics, Pergamon Press, Elmsford, NY, 1958.
32 M. Lozada-Cassou and E. Diaz-Herrera, in N. Ise and I. Sogami (Eds), Ordering and Organisation in Ionic Solutions, World Scientific, Singapore, 1988, p. 555.
33 E. Kamke, Differentialgleichungen, Vol. 1, Nauka, Moscow, 1976 (in Russian).
34 G.A. Korn and T.M. Korn, Mathematical Handbook, McGraw-Hill, New York, 1968.

35 H. Bateman and A. Erdelyi, Higher Transcendental Functions, Vol. 2, McGraw-Hill, New York, 1953.
36 A.P. Prudnikov, Y.A. Brychkov and O.I. Marichev, Integrals and Series-Higher Functions, Nauka, Moscow, 1983 (in Russian).
37 S. Nir and C.S. Vassilieff, in I.B. Ivanov (Ed.), Thin Liquid Films, Marcel Dekker, New York, 1988, p. 207.
38 J.B. Rijnbout, J. Phys. Chem., 74 (1970) 2001.
39 J.A. de Feijter, Thesis, University of Utrecht, 1973; J.A. de Feijter and A. Vrij, J. Colloid Interface Sci., 64 (1978) 269.
40 P.A. Kralchevsky, I.B. Ivanov and A.S. Dimitrov, Chem. Phys. Lett., 187 (1990) 129.
41 A.A. Ravdel and A.M. Ponomarjova (Eds), Brief Handbook of Physico-Chemical Properties, Khimia, Leningrad, 1983 (in Russian).
42 M. Abramovitz and I.A. Stegun (Eds), Handbook of Mathematical Functions, Dover, New York, 1965.
43 V.M. Muller, in B.V. Derjaguin (Ed.), Research in Surface Forces, Vol. 3, Consultants Bureau, New York, 1971, p. 236.

Appendix A: Equilibrium distribution of the charge density

Our aim is to specify the expressions for calculating some parameters of our model, which are connected with the ion density distribution. First we will briefly consider the case of the electric double layer, and then we will pay some attention to a modified version of the Poisson–Boltzmann theory of the thin liquid film.

Electric double layer

The parameters I_1, I_2, $\rho(0)$ and $n_2(0)$ can be calculated from the electrostatic potential $\Psi(z)$. The latter satisfies the Poisson–Boltzmann equation

$$\frac{d^2\psi}{dz^2} = \kappa_0^2 \sinh\psi, \qquad \psi = \frac{Ze\Psi}{k_B T} \tag{A1}$$

where κ_0 is given by Eqn (3.13). The boundary conditions are

$$\lim \psi = 0 \quad \text{and} \quad \lim(d\psi/dz) = 0 \quad \text{for} \quad z \to \infty \tag{A2}$$

From (A1)–(A2) we derive (see e.g. Ref. [6]):

$$\frac{d\psi}{dz} = -2\kappa_0 \sinh(\psi/2) \tag{A3}$$

$$\psi(z) = 4 \operatorname{arctanh}[\tanh(\psi_s/4)\exp(-\kappa_0 z)] \tag{A4}$$

where ψ_s is the surface potential (at $z = 0$). From the electroneutrality condition (the second Eqn (3.1)) one obtains [6]

$$(d\psi/dz)_{z=0} = \kappa_s, \qquad \kappa_s = -\frac{4\pi Ze\sigma}{\epsilon k_B T} \tag{A5}$$

The combination of Eqns (A3) and (A5) yields

$$\psi_s = -2 \operatorname{arcsinh}[\kappa_s/(2\kappa_0)] \tag{A6}$$

According to the Boltzmann equation

$$n_m(z) = n_0 \exp[(-1)^m \psi(z)], \qquad m = 1, 2 \tag{A7}$$

From Eqns (3.1) and (1.7) one obtains

$$\rho(z) = -2Zen_0 \sinh\psi(z) \tag{A8}$$

The integrals I_1 and I_2 are calculated numerically by substituting from Eqns (A4), (A6) and (A8) into Eqn (3.3). $n[(a + a_\infty)/2]$ is calculated from Eqns (A4), (A6) and (A7) by setting $z = (a + a_\infty)/2$. Finally, from Eqns (A7) and (A8) one obtains

$$n_2(0) = n_0 \exp\psi_s \tag{A9}$$

$$\rho(0) = -2Zen_0 \sinh\psi_s \tag{A10}$$

Thin liquid film

Let us choose the plane $z = 0$ to be located in the middle of the film, as shown in Fig. 2. In contrast with the conventional DLVO theory (see e.g. Refs [2 and 5]) we choose the potential to be zero in the middle of the film: $\psi = 0$ for $z = 0$. (As demonstrated below, this choice leads to simpler analytical expressions.) Then according to the Boltzmann equation, the ion concentrations read

$$n_m(z) = n_{m0} \exp[(-1)^m \psi(z)], \qquad m = 1, 2 \tag{A11}$$

where n_{10} and n_{20} are the concentrations of the counterions and co-ions at the middle of the film. Since the solution inside the film is supposed to be in electrochemical (Donnan) equilibrium with the bulk solution outside the film, one can write

$$n_{10} n_{20} = n_0^2 \tag{A12}$$

or alternatively

$$n_{10} = n_0/m^{1/2}, \qquad n_{20} = n_0 m^{1/2} \tag{A13}$$

where by definition

$$m = n_{20}/n_{10} \tag{A14}$$

In these notations the Poisson–Boltzmann equation reads

$$\frac{d^2\psi}{dz^2} = -\frac{\kappa_0^2}{m^{1/2}}[\exp(-\psi) - m\exp(\psi)] \tag{A15}$$

The boundary conditions are

$$\psi = 0 \quad \text{and} \quad d\psi/dz = 0 \quad \text{for} \quad z = 0 \tag{A16}$$

The electroneutrality condition yields

$$(d\psi/dz)_{z=h/2} = -\kappa_s \tag{A17}$$

(see Fig. 2 and Eqn (A5)). The first integration of Eqn (A15) along with Eqn (A16) yields

$$\frac{1}{y}\frac{dy}{dz} = \frac{\kappa_0}{m^{1/4}}[y - 1 + m(1/y - 1)]^{1/2} \tag{A18}$$

where by definition

$$y = \exp(-\psi) \tag{A19}$$

On integrating Eqn (A18) one obtains

$$z(y) = \frac{2}{\kappa_0} m^{1/4} F(\gamma|m), \qquad \gamma = \arcsin\left(\frac{y-1}{y-m}\right)^{1/2} \tag{A20}$$

where $F(\gamma|m)$ is an elliptic integral of the first kind [42]

$$F(\gamma|m) = \int_0^{\gamma} (1 - m\sin^2\theta)^{-1/2}\, d\theta \tag{A21}$$

We calculated $F(\gamma|m)$ by using the convenient method of the arithmetic-geometric mean; see Eqn (17.6.9) in Ref. [42]. At the film surface $z = h/2$, $y = y_s$ and Eqn (A20) yields

$$h(m) = \frac{4}{\kappa_0} m^{1/4} F(\gamma_s|m), \qquad \gamma_s = \arcsin\left(\frac{y_s - 1}{y_s - m}\right)^{1/2} \tag{A22}$$

An equation for determining y_s can be derived from Eqns (A17)–(A19):

$$p^2 m^{1/2} = y_s - 1 + m(1/y_s - 1), \qquad p = |\kappa_s/\kappa_0| \tag{A23}$$

From Eqn (A23) one obtains

$$y_s = \tfrac{1}{2}\{p^2 m^{1/2} + m + 1 + [(p^2 m^{1/2} + m + 1)^2 - 4m]^{1/2}\} \tag{A24}$$

Note that Eqns (A22) and (A24) represent h as an explicit function of m. The parameters

$$n_2(h/2) = n_0 m^{1/2}/y_s$$

and

$$\rho(h/2) = Zen_0\left(\frac{y_s}{m^{1/2}} - \frac{m^{1/2}}{y_s}\right) \tag{A25}$$

are also explicit functions of m. To find the last parameter, $n_2(s/4)$, from Eqn (A20) we first determine y as a function of z and then set $z = s/4$:

$$n_2\left(\frac{s}{4}\right) = \frac{n_0 m^{1/2}}{y(s/4)} = n_0 m^{1/2} - \frac{1 - \mathrm{sn}^2(x_4|m)}{1 - m\,\mathrm{sn}^2(x_4|m)} \tag{A26}$$

where $x_4 = \kappa_0 s/8$ and $\mathrm{sn}(x_4|m)$ is the elliptic sine of Jacobi, see e.g. Ref. [42].

To calculate the electrostatic excess free energy per unit area of the film we used the rigorous expression due to Muller [43]; see also Ref. [5]:

$$\Delta f_{el} = -\Pi_{el} h + 4n_0 k_B T I/\kappa_0 \tag{A27}$$

where

$$\Pi_{el} = n_0 k_B T[m^{1/4} - m^{-1/4}]^2 \tag{A28}$$

is the electrostatic component of the disjoining pressure and

$$I = 4(\xi_\infty^2 + 1)^{1/2} - 4 + 4|\xi_\infty| \ln\left|\frac{\xi_0 + (\xi_0^2 + 1)^{1/2}}{\xi_\infty + (\xi_\infty^2 + 1)^{1/2}}\right| - 2\int_{\xi_m^2}^{\xi_0^2} \left[\frac{s - \xi_m^2}{s(s+1)}\right]^{1/2} ds \tag{A29}$$

where

$$\xi_m = -\sinh(\psi_m/2), \qquad \xi_\infty = -\sinh(\psi_\infty/2),$$

$$\xi_0 = -\sinh(\psi_0/2) \tag{A30}$$

$$\psi_m = \tfrac{1}{2}\ln m, \qquad \psi_\infty = -2\,\mathrm{arcsinh}(p/2),$$

$$\psi_0 = \psi_m - \ln y_s \tag{A31}$$

and y_s is given by Eqn (A24). The integral in the right-hand side of Eqn (A29) we calculated numerically.

The algorithm of our computer calculations is given in Appendix B below.

Appendix B: Algorithm for calculating the film excess free energy and the disjoining pressure

Since the number of parameters and equations in this work turned out to be large, we propose below an algorithm for calculating the excess free energy per unit area of the film Δf and the disjoining pressure Π.

1. Input parameters: area per unit surface charge A (cm^2), bulk electrolyte concentration n_0 (cm^{-3}), number of charges per ion Z, temperature T (K), dielectric permittivities ϵ and ϵ_1, width of the Stern layer w (cm).

2. Calculation of κ_0 from Eqn (3.13), κ_s from Eqn (A5), ψ_s from Eqn (A6), p from Eqn (A23) and $\sigma = \pm e/A$ ($e = 4.803 \cdot 10^{-10}$ CGSE units); the sign of σ depends on whether the surface is positively or negatively charged.

3. The integrals I_1 and I_2 are calculated by numerical integration from Eqns (A4), (A6), (A8) and (3.3).

4. Calculation of $n_2(0)$ from Eqn (A9), $\rho(0)$ from Eqn (A10); a, a_∞, ρ^{I} and ρ^{II} from Eqns (3.5)–(3.7); n_1^{I} and n_2^{I} from Eqn (3.9); n_1^{II} and n_2^{II} from Eqns (3.10)–(3.11); κ_I and κ_{II} from Eqn (3.12).

5. $n_2[(a+a_\infty)/2]$ is calculated by setting $z = (a+a_\infty)/2$ in Eqn (A7) and by using Eqns (A4) and (A6).

6. Some value of the parameter m is input. Each value of m corresponds to a value of the film thickness h (see point 7) $0 < m < 1$, $0 < h < \infty$. By varying m one can calculate the dependence of Δf and Π on the film thickness h.

7. y_s is calculated from Eqn (A24), γ_s and the film thickness h from Eqn (A22).

8. $n_2(s/4)$ is calculated by means of Eqn (A26); to calculate $\mathrm{sn}(x_4|m)$ we used Eqn (16.4.4) in Ref. [42].

9. $n_2(h/2)$ and $\rho(h/2)$ are calculated from Eqn (A25); $\hat{n}_1^{Y}$ and $\hat{n}_2^{Y}$ from Eqns (3.18)–(3.21) and $\hat{\kappa}_Y$ from Eqn (3.23); Y = I, II.

10. Δu_{cor}^{I} and Δf_{cor}^{I} are calculated from Eqns (4.34)–(4.35). The integrals with respect to k and T are calculated numerically. For each value of k one determines λ, α, b, c and τ from Eqns (4.7), (4.13) and (4.19); then $H^{I}(b, \beta, \nu)$ and $H^{I}(b_\infty, \beta_\infty, \nu_\infty)$ are calculated from Eqns (4.22)–(4.25) and (4.30). When $w = 0$ one can use Eqn (4.55) instead of Eqn (4.35).

10*. When the film is formed between two electro-conductors (Dirichlet problem) we use Eqns (4.57)–(4.67) to calculate Δf_{cor}.

11. Δu_{cor}^{II} and Δf_{cor}^{II} are calculated from Eqns (4.46)–(4.47). The integral term is calculated numerically. For each value of k one determines λ, α, b, c, τ and β from Eqns (4.7), (4.13) and (4.19). The function $H^{II}(c, \alpha, \lambda)$ and $H^{II}(c_\infty, \alpha_\infty, \lambda_\infty)$ are calculated from Eqns (4.39)–(4.40).

12. The excess free energy due to ionic correlations is determined by using Eqn (4.48).

13. The excess free energy due to the van der Waals forces, Δf_{vw} is calculated from Eqn (4.50) with h_w given by Eqn (5.5).

14. The excess free energy due to the electrostatic forces, Δf_{el}, is calculated from Eqn (A27) along with Eqns (A28)–(A31).

15. The total excess free energy, Δf, at a given film thickness h is calculated from Eqn (5.1). By varying the parameter m (point 6 above) with a given step, one calculates $\Delta f = \Delta f(m)$, $h = h(m)$ and then one can draw the plot of Δf vs h.

16. The disjoining pressure isotherm $\Pi(h)$ is calculated in accordance with Eqn (5.3) by numerical differentiation of the plot of Δf vs h.